

# Faraday-waves contact-line shear gradient induces streaming flow and tracers' self-organization: from rotating rings to spiral galaxy-like patterns

Héctor Alarcón,<sup>1,2, a</sup> Matías Herrera,<sup>3</sup> Nicolas Périnet,<sup>2</sup>  
Nicolás Mujica,<sup>2</sup> Pablo Gutiérrez,<sup>1, b</sup> and Leonardo Gordillo<sup>3, c</sup>

<sup>1</sup>*Instituto de Ciencias de la Ingeniería, Universidad de O'Higgins,  
Av. Libertador Bernardo O'Higgins 611, Rancagua, Chile*

<sup>2</sup>*Departamento de Física, Facultad de Ciencias Físicas y Matemáticas,  
Universidad de Chile, Av. Blanco Encalada 2008, Santiago, Chile*

<sup>3</sup>*Departamento de Física, Universidad de Santiago de Chile,  
Av. Ecuador 3493, Estación Central, Santiago, Chile*

In this letter we experimentally demonstrate self-organization of small tracers under the action of longitudinal Faraday waves in a narrow container. We observe a steady current formation dividing the interface in small cells given by the symmetries of the Faraday wave. These streaming currents are rotating in each cell and their circulation increases with wave amplitude. This streaming flow drives the tracers to form patterns, whose shapes depend on the Faraday wave's amplitude: from low to high amplitudes we find dispersed tracers, a narrow rotating ring and a spiral galaxy-like pattern. We first describe the main pattern features, and characterize the wave and tracers' motion. We then show experimentally that the main source of the streaming flow comes from the time and spatial dependent shear at the wall contact line, created by the Faraday wave itself. We end by presenting a 2D model that considers the minimal ingredients present in the Faraday experiment, namely the stationary circulation, the stretching component due to the oscillatory wave and a steady converging field, which combined produce the observed self-organized patterns.

PACS: 89.75.Kd: Pattern formation in complex systems; 47.55.np Contact lines; 47.35.Bb Gravity waves

The free surface of liquids is usually covered by particles. In the ocean these can include impurities, living organisms, nutrients, seeds, garbage or even bubbles. Due to ocean's continuous motion, these *tracers* are constantly arranging themselves as they respond to sea waving [1]. In more controlled, laboratory conditions, there are several mechanisms that can influence tracers' assembly into patterns. Formation of patterns has been attributed to particles properties, as wetting [2–5], filling fraction of the surface [3, 6], or inertial effects [7]. But tracers can also be steered by underlying flows [8–11]. Even in controlled settings as standing Faraday waves, several mechanisms lead to fluid motion decoupled from the periodicity of the waves [12, 13], where tracers' motion becomes difficult to predict. An example of the difficulties faced when predicting motion is the simple case of propagating waves generated by an oscillating plunger, which has shown a surprising flow reversal when cross-wise waves form [14]. In particular, walls play a relevant role because dynamic wetting between liquid and moving walls determines flow boundary conditions [15–18] and strongly influences dissipation [19–21].

In this letter, we identify a new mechanism leading to streaming flows on standing Faraday waves: a space-time dependent shear, produced at the oscillatory liquid-wall contact line. The steadiness and localization of the induced streaming flow, drives surface tracers to an exotic self-organization, documented and explained here for the first time.

This letter is organized as follows: we start by present-

ing the Faraday-waves setup, where we observe tracer self-organized patterns, which we describe. We continue by focusing in measurements of the streaming flow, which is, as we hypothesize, produced by a shear gradient on the contact line. We replicate this flow with a simplified setup that only engenders shearing of the liquid at the solid wall. We finish by presenting a 2D model that considers the minimal ingredients present in the Faraday experiment, which reproduces the observed patterns.

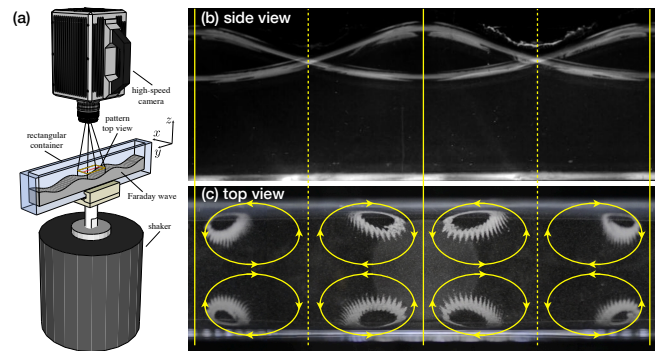


Figure 1. Experimental setup and spiral galaxy-like patterns. (a) An electromechanical shaker vibrates vertically the acrylic container with a water-surfactant liquid mixture and a small amount of silver-coated hollow glass micro-spheres. Side (b) and top (c) views of the patterns observed on a single Faraday wavelength. Solid (dashed) lines indicate anti-nodes (nodes). The observed streaming flow is sketched as arrowed ovals in (c).

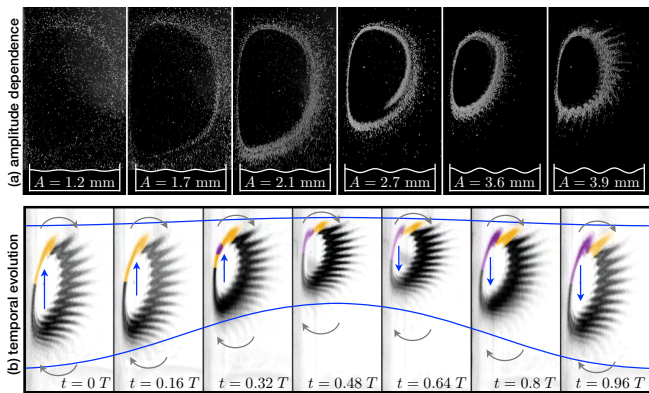


Figure 2. Elementary spiral galaxy-like pattern. (a) Pattern at a given phase for various wave amplitudes  $A$ . (b) Breathing motion during a single oscillation (gray scale was inverted for clarity); the formation of a new arm is highlighted in purple.

*Experiment on Faraday waves.* The experimental setup used to produce Faraday waves is a rectangular acrylic container with interior dimensions of  $26.5 \times 280 \times 55 \text{ mm}^3$  attached to an electromechanical shaker allowing vertical vibrations [Fig.1(a)]. The container is filled up to 30 mm deep with an aqueous solution of 218 g of distilled water and 2 ml of Kodak Photo-Flo, used as wetting agent [22], and sprinkled homogeneously with 0.1 mg of  $10 \mu\text{m}$  diameter silver-coated hollow glass micro-spheres, whose mass density is  $\rho = 1.4 \text{ g cm}^{-3}$  (Dantec Dynamics, S-HGS). The container vibrates sinusoidally  $z(t) = a \sin(\omega_d t)$ , at the driving amplitude  $a$  and the fixed frequency  $f_d = \omega_d/2\pi = 8.30 \text{ Hz}$ . This driving induces super-critical (non-hysteretic) Faraday waves at  $f = f_d/2 = 4.15 \text{ Hz}$ , above a normalized critical acceleration amplitude  $\Gamma_c = a_c \omega_d^2/g = 0.144 \pm 0.001$  ( $g$  is the gravitational acceleration). Under these experimental conditions, the observed stationary Faraday wave forms a (3,0)-mode, i.e. three wavelengths in the long-wise direction with no crosswise component.

To characterize the flow due to Faraday waves, we measured simultaneously the position of the tracers and the amplitude of the waves. In order to visualize and track the tracers, we set a camera above the container and a focused razing horizontal light from the side. The recording frequency is 100 fps with a  $1920 \times 1080 \text{ pix}^2$  resolution. The local height of Faraday waves is simultaneously measured from a side view using a tilted mirror [Fig. 1(b)].

*Flow structure and tracers' self-organization.* As soon as Faraday waves emerge, tracers begin to circulate inside cells limited in the  $x$ -direction by the central plane of the container and the walls, and in the  $y$ -direction by node and anti-node planes, as indicated in Fig. 1(c). The circulation is steady and its origin will be discussed later. Cells adjacent to antinodes or center lines shelter identical but counter-rotating patterns, as shown in Fig. 1(c).

Near walls, tracers always go from node to antinode [23]. This circulation-cell structure is compatible with previous streaming flow observations [17].

Tracers display four organization regimes depending on the Faraday wave amplitude  $A$ , as shown in Fig. 2(a) and [23]: 1) for  $A \leq 1.5 \text{ mm}$  the rotating tracers spread more or less homogeneously over each cell, 2) above  $A \approx 1.5 \text{ mm}$ , tracers in each cell shrink into a rotating ring, 3) for  $A > 2.8 \text{ mm}$ , the rotating ring sharpens and exhibits *arms* in a shape that is reminiscent of spiral galaxies. The arms form after each wave cycle and their length increases with  $A$ . 4) Finally, for  $A > 4.3 \text{ mm}$ , arms become very long and oscillate in a time scale much larger than the one of the Faraday waves (not shown in Fig. 2).

In streaming galaxy-like patterns, one new arm emerges in each oscillation period. The arm formation can be observed along a representative cycle shown in Fig. 2(b). In one hand, the pattern compresses and stretches periodically, as a slave mode of the free surface oscillation. This induces a back-and-forth motion during the oscillation period, as schematized with vertical blue arrows in Fig. 2(b). On the other hand, the steady streaming slowly rotates the pattern, as shown with the curved arrows in the same figure. Arms appear in the stage of surface compression: tracers near the wall (emphasized in purple) are traveling faster than their counterparts near the anti-node (in yellow). Therefore, fluid parcels fold, giving birth to an arm.

In order to evaluate the role of the particle nature of tracers in the pattern formation, we ran the experiment using soluble dyes (ink) and the patterns remained. Moreover, increasing the concentration of tracers by a factor 5 keeps the observed patterns unaltered. These observations demonstrate that the patterns are generated by the flow itself, and tracers interaction or buoyancy are not relevant for their emergence, contrary to what was observed in previous experiments with larger particles [2, 3].

*Steady Streaming.* In our Faraday experiments we observe a steady circulation, as schematized in Fig.1(c). Due to their small size, tracers follow fluid parcels. To characterize their displacement, we use image cross-correlation. However, due to high wave amplitudes, large in-plane deformation limits global measurements. We specifically refer to the interface stretching that occurs due to the longitudinal wave. Therefore, we focused on 8 small sections of the ring formed by tracers, shown in Fig. 3(a). We track the longitudinal in-plane displacement due to the Faraday wave as in a Lagrangian frame of reference. The velocity of this frame of reference is time dependent and obtained by linear interpolation along  $y$  between the velocities of the two extremities of the ring. Then we compute image cross-correlation between small windows that follow this frame of reference. The total velocity is then deduced from the prescribed Lagrangian displacement plus the one measured from image cross-

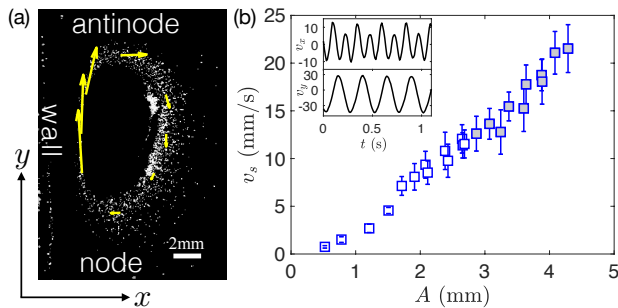


Figure 3. (a) Tracer velocities around a unit-cell rotating ring, for  $A = 2.1$  mm. Streaming velocities, shown as yellow arrows, are measured at 8 different locations around the ring, being much larger close to the wall. (b) Streaming speed averaged at the three points near the wall as a function of the wave amplitude. Solid points correspond to measurements with the arms well developed in the circulating ring. Inset: examples of instantaneous velocity components at a given point around the ring.

correlation. Figure 3(a) shows an instantaneous picture, and the inset of Fig. 3(b) shows the time evolution of the  $x$ - and  $y$ -velocity components of a single point near the wall.

Temporal evolution in  $v_y$  shows a sub-harmonic oscillation, while  $v_x$  exhibits a harmonic mode. While the Faraday wave is the dominant motion along  $y$ , the  $x$ -direction is more sensitive to meniscus waves. Both velocity components have a well-defined non-zero time-average, corresponding to the steady streaming. To evaluate this magnitude in function of  $A$ , we define  $v_s$  as the average speed between the three points near the wall. The main panel of Fig. 3(b) shows that  $v_s$  increases first quadratically, then nearly linearly with  $A$ .

The final, and most remarkable feature of the streaming flow is its heterogeneity along the ring. Indeed, Fig. 3(a) shows that the velocity is around 6 times larger near the walls than close to the container's center line. Therefore, near the wall, the liquid experiences a large acceleration linked to a strong shear gradient. For standing waves, due to the dynamical variation of the surface elevation between nodes and antinodes, a space-time dependent shear gradient is ubiquitous whenever walls are present. Are circulating streaming flows a generic feature when a space-time variable shear gradient is exerted on a liquid-solid-air contact line? We will answer this by isolating the effect of the oscillatory shear gradient.

*Rotating disk experiment.* A circular disk (of radius  $R = 40$  mm) rotates periodically between angles  $\theta$  and  $-\theta$ , driven by a stepper motor (see Fig. 4(a)). The disk is partially immersed in water up to its center, so that any point oscillates with an amplitude  $r\theta$ , with  $r$  the distance from the center (see Fig. 4(a)), and with a maximum arc amplitude  $A = R\theta$ . We limited  $A$  to 8 mm in order to avoid sloshing motion. Oscillation frequency  $f$  is set

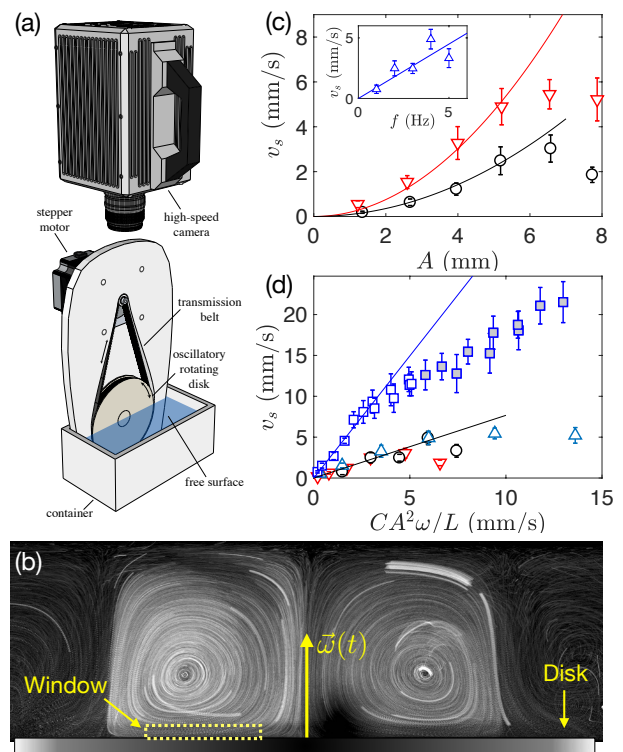


Figure 4. (a) Schematic illustration of the rotating disk setup. (b) Top view of the observed streaming pattern,  $A = R\theta = 2.67$  mm and  $f = 2$  Hz. The PTV measurement window is shown as dashed rectangle. (c) Streaming speed as function of disk oscillation amplitude  $A$ , for  $f = 2$  Hz ( $\nabla$ ) and  $f = 4$  Hz ( $\circ$ ). Inset:  $v_s$  linear frequency dependence for fixed  $A$ . (d)  $v_s$  as function of  $C\omega A^2/L$ , with  $L = R$  and  $C = 0.35$  for the disk, and  $L = \lambda$  and  $C = 2.5$  for Faraday data. The disk data collapses on a single curve, showing a saturation at higher values. For both experiments an  $A^2$  scaling is observed for the lower amplitude regime, shown as straight lines as guides to the eye.

independently. The disk is made of acrylic, having similar wetting properties as the container used for Faraday waves. The disk oscillatory motion, therefore, simulates the spatio-temporally varying triple-line position distinctive of Faraday waves.

Fig. 4(b) presents a digitally overexposed image, revealing flow streamlines. The result is striking, as it shows a steady circulation reminiscent of the one observed in the Faraday experiment for low amplitudes. In order to further characterize this steady streaming, we measured the spatial average streaming speed  $v_s$  in a window close to the disk, as shown in this figure. Here, because motion is much slower than in the Faraday experiment, we are able to perform simple Particle Tracking Velocimetry (PTV) measurements on tracers that are detected. The streaming speed is then computed as a time-spatial average from individual tracer measurements. We performed measurements for fixed  $f$  increasing  $A$ , and also for fixed  $A$  increasing  $f$ . We observe

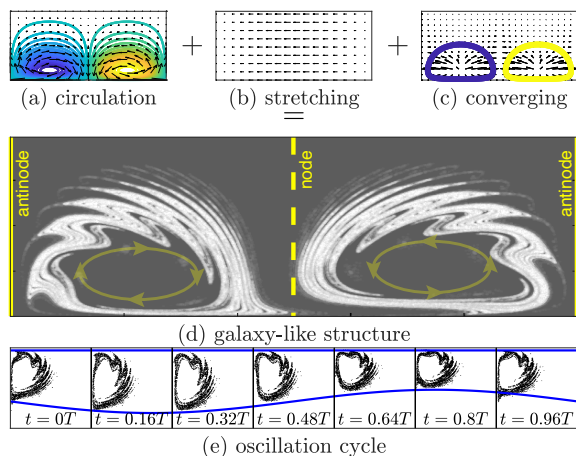


Figure 5. (a) Steady circulation, (b) periodic stretching and (c) a steady converging field featured by a ring, are the basic ingredients to generate galaxy-like structures. The superposition of the velocity fields allows agglomeration of particles (d) and similar dynamics, including rotation, breathing and formation of arms in every cycle (e) as those that emerge in patterns on Faraday waves.

a linear increase of  $v_s$  with  $f$ , and a quadratic dependence on  $A$ , with a saturation at the highest values [Fig. 4(c)]. When plotting  $v_s$  in function of  $A^2\omega/R$ , all disk measurements collapse on a single curve (see Fig. 4(d)). The consistency of both scaling laws at low amplitudes allows us to conclude that the circulation comes from the shear gradient of vertical velocity at the walls, similar to what was proposed in [17, 24], but specifically applied to the contact line. Indeed, the data is consistent with  $v_s \propto \langle w_{\sim} \partial_y w_{\sim} \rangle / (2\pi f)$ , where the vertical velocity component of the contact line at the wall is  $w_{\sim} = 2\pi f A \sin(ky) \cos(2\pi ft)$  for Faraday waves and  $w_{\sim} = 2\pi f A y \cos(2\pi ft) / R$  for the disk. Here, the brackets  $\langle \rangle$  stand for the spatial and temporal average in each case. The constant  $C$  used in Fig. 4(d) is the result of the numerical factors for each case, considering also the spatial averaging. The law  $v_s \propto \langle w_{\sim} \partial_y w_{\sim} \rangle / (2\pi f)$  also gives an explanation to the generation of eddies on the crosswise waves in [14], which share the common feature of sheared oscillating contact lines. It also consistently predicts that nodes/antinodes generate inward/outward jet streams in such configuration.

*Simple advection model.* The experiment with the oscillatory rotating disk successfully isolates the gradient of shear exerted on the contact line as it oscillates on the wall. It clearly shows that the primary origin of the circulation of the observed patterns in Faraday waves is not the presence of the wave itself, but the shear gradient along the contact line. The question that naturally arises is whether it is possible to go further with a model that is not only able to predict a rotating velocity field but also complex galaxy-like structures.

We have concluded that there are three fundamental features required for the formation of galaxy-like structures, which can be put into a simple 2D phenomenological advection model. These are:

1. *A steady circulation.* To build a velocity field that has the features observed in Faraday cells, we consider a modification of the classic flow of a 2D rectangular cavity driven by a moving wall. Instead of imposing a uniform velocity at one of the boundaries of the cavity, we imposed a non-uniform velocity,  $\propto -\sin(2ky)$  in the lower boundary at  $x = 0$ , to mimic the effect of the sheared contact line. Free-slip boundary conditions are applied on the rest of the boundaries as they correspond to the symmetry planes of the Faraday-wave cells. The streamlines due to the presence of this flow can be calculated analytically [23] and are shown in Fig. 5(a).

2. *A periodic stretching.* Figure 2 shows that the structures undergo periodic stretching in time. To account for this, we added an oscillatory field given by  $v(x, y, t) = -\epsilon \sin ky \cos \omega t$ , where  $\epsilon$  is the amplitude of the deformation due to the main motion of the stationary Faraday wave as shown in Fig. 5(b).

3. *A steady converging field.* This flow accumulates the particles into a ring (see Fig. 5(c)). To account for this, we took the rotating velocity field and manipulated it to generate a secondary flow that converges particles into one of its streamlines [23].

We ran simple numerical simulations in which an initially random distribution of particles is advected by the superposition of these three velocity fields. As shown in [23], particles agglomerate in structures that are incredibly similar to those observed on Faraday waves as shown in Fig. 5(d). The model captures successfully very specific and complex features of the motion of the structures: the breathing dynamics [Fig. 5(e)], the mechanism for generation of arms in each period and a gradual decrease of the length of the arms as they approach the wall.

In conclusion, we have found experimentally that the flow at the interface of Faraday waves undergoes a transition from circulating rings to spiral-like galaxies as the wave amplitude increases. The observed galaxy arms are created at each period due to the strong shear gradient at the wall and the fast deceleration of the circulating ring into the bulk of the interface, away from the walls. We demonstrated that the main source of the streaming flow comes from the time and spatial dependent shear on the contact line at the wall boundary, induced by the Faraday wave itself. The streaming flow is quite generic, as a similar circulation flow is observed in the oscillating rotating disk experiment. Both experiments follow the scaling  $v_s \propto \langle w_{\sim} \partial_y w_{\sim} \rangle / (2\pi f)$  for the average streaming speed near the wall, where  $w_{\sim}$  is the contact-line vertical velocity component on the wall. The proposed scaling law provides also an explanation to the eddies and jet streams documented in Punzmann *et al.* [14], setting the

basis for the understanding of flow reversal on propagating waves. Finally, we propose a simplified 2D model that considers the minimal ingredients that are necessary to obtain spiral-galaxy-like patterns, namely the stationary circulation, the stretching component due to the oscillation and a steady converging field. The model imitates the patterns observed experimentally in many regards. As a perspective, this flow, which is periodic with a nonlinearly generated stationary component, is an interesting system for studying Lagrangian coherent structures [1, 25], specially considering that the stirring process ends with a complex pattern of tracers with a high degree of spatiotemporal organization in a rather simple experimental configuration.

H. A. acknowledges the support of Fondecyt postdoctoral program, grant 3160341. L.G., P.G. and N.M. acknowledge support of ANID through the Fondecyt grants N°11170700, N°11191106 and N°1180636, respectively.

---

<sup>a</sup> [hector.alarcon@uoh.cl](mailto:hector.alarcon@uoh.cl)

<sup>b</sup> [pablo.gutierrez@uoh.cl](mailto:pablo.gutierrez@uoh.cl)

<sup>c</sup> [leonardo.gordillo@usach.cl](mailto:leonardo.gordillo@usach.cl)

- [1] G. Haller, *Annu. Rev. Fluid Mech.* **47**, 137 (2015).
- [2] G. Falkovich, A. Weinberg, P. Denissenko, and S. Lukaschuk, *Nature* **435**, 1045 (2005).
- [3] C. Sanli, D. Lohse, and D. van der Meer, *Phys. Rev. E* **89**, 053011 (2014).
- [4] M.-J. Dalbe, D. Cosic, M. Berhanu, and A. Kudrolli, *Phys. Rev. E* **83**, 051403 (2011).
- [5] D. Vella, *Annu. Rev. Fluid Mech.* **47**, 115 (2015).
- [6] M. Berhanu and A. Kudrolli, *Phys. Rev. Lett.* **105**, 098002 (2010).
- [7] F. Santamaria, G. Boffetta, M. Martins Afonso, A.azzino, M. Onorato, and D. Pugliese, *Europhys Lett* **102**, 14003 (2013).
- [8] G. Boffetta, J. Davoudi, B. Eckhardt, and J. Schumacher, *Phys. Rev. Lett.* **93**, 134501 (2004).
- [9] J. R. Cressman, J. Davoudi, W. I. Goldburg, and J. Schumacher, *New Journal of Physics* **6**, 53 (2004).
- [10] P. Gutiérrez and S. Aumaître, *Eur. J. Mech. B* **60**, 24 (2016).
- [11] S. Lovecchio, C. Marchioli, and A. Soldati, *Phys. Rev. E* **88**, 033003 (2013).
- [12] N. Francois, H. Xia, H. Punzmann, S. Ramsden, and M. Shats, *Phys. Rev. X* **4**, 021021 (2014).
- [13] S. V. Filatov, V. M. Parfenyev, S. S. Vergeles, M. Y. Brazhnikov, A. A. Levchenko, and V. V. Lebedev, *Phys. Rev. Lett.* **116**, 054501 (2016).
- [14] H. Punzmann, N. Francois, H. Xia, G. Falkovich, and M. Shats, *Nature Physics* **10**, 658 (2014).
- [15] C.-L. Ting and M. Perlin, *J. Fluid Mech.* **295**, 263 (1995).
- [16] L. Gordillo and N. Mujica, *J. Fluid Mech.* **754**, 590 (2014).
- [17] N. Périnet, P. Gutiérrez, H. Urra, N. Mujica, and L. Gordillo, *J. Fluid Mech.* **819**, 285 (2017).
- [18] Y. Huang, C. L. P. Wolfe, J. Zhang, and J. Q. Zhong, *J. Fluid Mech.* **895**, A1 (2020).
- [19] L. Jiang, M. Perlin, and W. W. Schultz, *Phys. Fluids* **16**, 748 (2004).
- [20] L. Gordillo and M. A. Garcia-Ñustes, *Phys. Rev. Lett.* **112**, 164101 (2014).
- [21] B. Dollet, É. Lorenceau, and F. Gallaire, *Phys. Rev. Lett.* **124**, 104502 (2020).
- [22] J. Wu, R. Keolian, and I. Rudnick, *Phys. Rev. Lett.* **52**, 1421 (1984).
- [23] See Supplemental Material at ... for experimental videos, technical details and numerical simulations of the advection model.
- [24] J. A. Nicolás and J. M. Vega, *Fluid Dyn. Res.* **32**, 119 (2003).
- [25] M. Farazmand and G. Haller, *Chaos* **22**, 013128 (2012).